Nanoscale optical microscopy in the vectorial focusing regime

K. A. SERRELS, E. RAMSAY, R. J. WARBURTON AND D. T. REID*

Ultrafast Optics Group, School of Engineering and Physical Sciences, Heriot-Watt University, Riccarton, Edinburgh EH14 4AS, UK
***e-mail: d.t.reid@hw.ac.uk**

Published online: 9 March 2008; doi:10.1038/nphoton.2008.29

It has been known since 1959 that the focal-plane intensity distribution produced by focusing polarized light with a high-numerical-aperture lens should be highly asymmetric[1]. Remarkably, the consequences of this fundamental effect in direct image acquisition have remained unexploited, although vectorial effects have been observed in the contexts of free-space focusing[2], molecular fluorescence[3] and photolithography[4]. By using extreme-numerical-aperture (values of 3.5), solid-immersion microscopy[5–7] we have obtained images of a silicon integrated circuit showing, for the first time, the dramatic influence of polarization on their spatial resolution, with values from 100 nm to 250 nm. Our data show that polarization-sensitive imaging can substantially surpass the scalar diffraction limit embodied by classical formulae such as Sparrow's criterion. Such performance will have an impact on activities such as integrated-circuit failure analysis, where optical inspection faces serious challenges from the sub-100-nm feature sizes routinely used in production devices.

Solid immersion lens (SIL) imaging represents one of the highest resolution techniques available for subsurface microscopy and optical data storage[5]. In particular, by using a super-SIL (ref. 6) geometry for subsurface microscopy it is possible to achieve a numerical aperture (NA) approaching the refractive index of the substrate material[7]. We recently reported diffraction-limited subsurface imaging by using a super-SIL to obtain a two-photon optical beam induced photocurrent (TOBIC) (ref. 8) image of a silicon integrated circuit[9], achieving a resolution of <170 nm with an illumination wavelength of 1,530 nm (ref. 10). Under such high-NA conditions, the resulting focal-plane intensity distribution is strongly asymmetric and cannot be described correctly by scalar diffraction theory because the polarization direction of the incident light must be taken into account. The vectorial theory of Richards and Wolf[1] addresses this problem, and here we report the first example (to our knowledge) of imaging under conditions where the vectorial nature of light leads to substantial differences in the resolutions obtained for opposite polarization states.

To investigate the role of polarization under high-NA conditions we implemented TOBIC imaging using the experimental arrangement shown in Fig. 1a. Two-photon excitation was achieved through the use of a 1,530-nm mode-locked erbium-fibre laser with a linearly polarized output beam that overfilled an objective lens of NA = 0.55. A half-wave plate positioned before the objective lens allowed the polarization direction of the beam to be controlled. The laser generated 160-fs pulses at a repetition frequency of 30 MHz with an average output power of 75 mW (peak, 15.6 kW), and its output was focused by the objective lens through a silicon super-SIL into the device under test. We used a silicon super-SIL based on the prescription given by Ippolito *et al.*[11] for stigmatic imaging, which states that a structure buried at a depth X can be imaged using a super-SIL whose vertical thickness is $R(1+1/n)-X$, where R is the SIL radius of curvature and n is its refractive

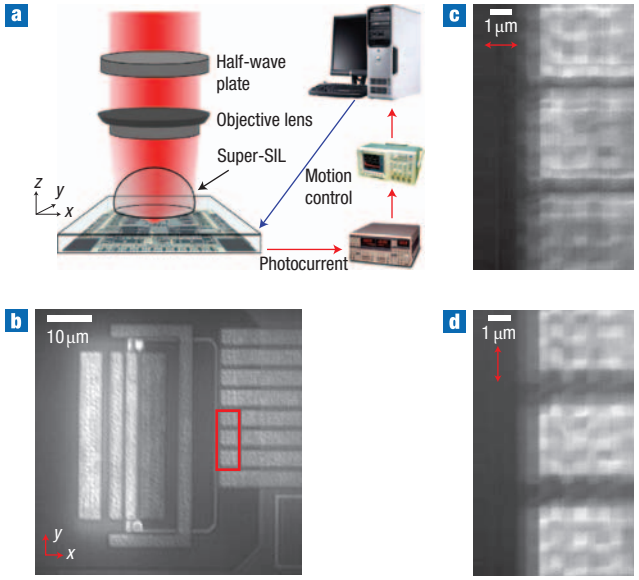

Figure 1 Polarization-sensitive subsurface imaging of a silicon integrated circuit. a, Experimental arrangement showing computer-aided control and acquisition of the image. **b**, Wide field-of-view TOBIC image (800-nm sampling resolution) recorded for navigation purposes and indicating the region (red box) at the end of three finger-like structures imaged at maximum resolution. **c**,**d**, TOBIC images of the boxed region showing three 3×3 grids of tungsten vias obtained under the linear polarizations indicated by the red arrows. Lighter image rendering indicates a higher TOBIC photocurrent and the left sides of the detailed finger images have been padded with black to allow the scale bar to appear on a uniform background. The PSF is narrower in the direction normal to the polarization vector, therefore the gaps between the fingers are better resolved when the polarization vector lies along the finger edges (**c**).

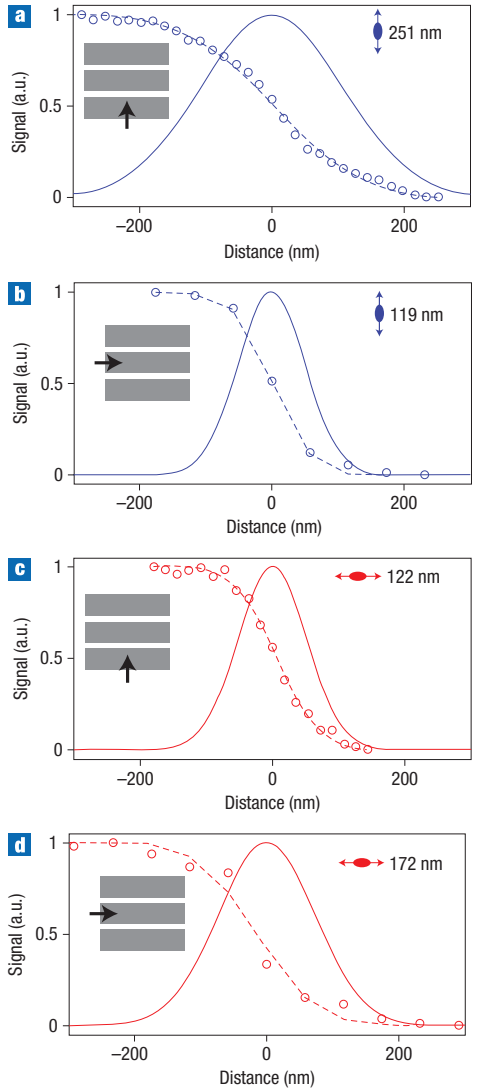

Figure 2 Resolution measurements under different polarization conditions. **a**,**b**, Line cuts through the detailed images shown in Fig. 1d, which was recorded for incident light with a wavelength of 1,530 nm polarized parallel to the *y* direction (as defined in Fig. 1b). **c**,**d**, Equivalent data recorded for the image acquired with the orthogonal polarization state, which was parallel to the *x* direction (as in Fig. 1c). The polarization direction in each panel is indicated by the blue or red two-way arrows, and the indicative focal-spot shape is shown by the ellipse between the arrows heads, together with the PSF FWHM inferred from a gaussian fit to the data. The scan direction of the beam relative to the sample is indicated by the black arrow.

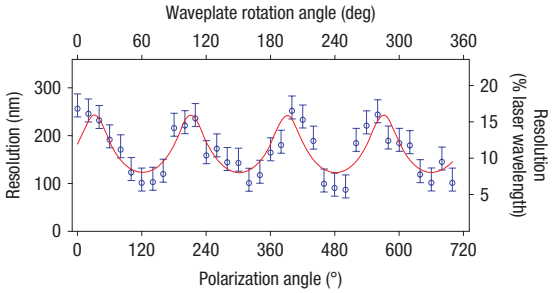

Figure 3 Dependence of measured resolution values on polarization direction. The resolution measurements were recorded at half-wave plate angular intervals of 10° and show a 180° period in the electric-field polarization direction, which is a result of the ellipticity of the focal spot. A least-squares fit to the data (solid curve) implies polarization-dependent minimum and maximum resolutions of 122 nm and 240 nm, respectively (a ratio of 1.97), with a standard deviation of 31 nm (upper error bars) from the fitting function. The measurement error associated with each data point was around ±17 nm (lower error bars). The laser wavelength was 1,530 nm.

index[7]. When this condition is fulfilled, no spherical aberration is introduced into the image. The sample was a CMOS silicon flip-chip fabricated using 0.35-μm technology and had an exposed silicon substrate that had been optically polished to a thickness of 100 μm. A photocurrent was generated and collected at the device terminals through two-photon carrier generation at the device layer of the chip[8] and acquired using narrow-band amplification and lock-in detection using a digital oscilloscope and personal computer. The device under test was mounted on a computer-controlled motorized three-axis translation stage, which had a minimum physical stepping increment along each axis of 100 nm, corresponding to a minimum optical stepping interval of ∼8.3 nm (ref. 7).

A striking example of the different imaging outcomes obtained by using orthogonal polarization states is shown in Fig. 1b–d. We performed high-resolution TOBIC imaging on the region of the device indicated by the red box in Fig. 1b, which comprised n-type silicon fingers bordered by a metallization region. The tip of each silicon finger contained a 3 × 3 matrix of tungsten vias—small metal wires that interconnect two layers of an integrated circuit—that interconnected the silicon device layer with the first metallization layer. The detailed images shown in Fig. 1c,d have a 13 μm × 6.5 μm field-of-view and a vertical (horizontal) optical sampling interval of 18 nm (58 nm). The polarization state used for image acquisition is indicated by the red arrow, and vectorial focusing theory predicts that the focal spot is elongated along this direction. An immediate consequence of the focal spot asymmetry is obvious in the panels, in that where the polarization direction lies along the gap between the fingers (Fig. 1c), the edges appear sharper and more clearly resolved. In contrast, when the polarization direction lies in the opposite direction (Fig. 1d), the edges between the fingers are blurred and the gap between the fingers appears to be wider. To study this effect in a quantitative way we examined the transition in the image signal as the beam was scanned across the horizontal and vertical edges of the fingers. The line cuts through the image data are shown in Fig. 2 (open circles) and were fitted to a gaussian error function to determine the width of the point-spread function (PSF) in each direction and for each polarization state. The results show a twofold difference in resolution for data acquired with opposite polarization states when scanning across the gaps between neighbouring fingers (122 nm and 251 nm). A smaller polarization-dependent difference (119 nm versus 172 nm) is observed for data obtained by scanning into the tip of a finger, and this is attributed to the different metal and dielectric environments encountered by the beam in different regions of the device. Scanning into an isolated edge (the finger tip) should give a different result to scanning across closely neighbouring edges because, for close edges, the optical field interacts with the two edges simultaneously, modifying the image obtained.

The asymmetry of the tightly focused spot was also investigated by acquiring multiple resolution measurements over the same edge

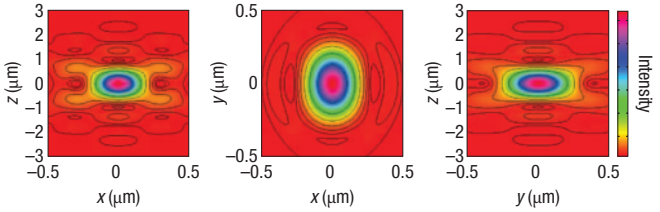

Figure 4 Calculated time-averaged focused intensity distribution of 1,530-nm light focused by a super-SIL into a silicon substrate. a, Section through the $x-z$ plane, where z is the optical axis. **b**, Section through the focal plane ($x-y$), showing the rotational asymmetry of the focal spot. **c**, Section through the $y-z$ plane. The incident polarization is parallel to the y axis. The colour map is linear in intensity and adjacent contour lines are separated by a factor of two. In the $x-y$ plane the calculated spot has an ellipticity of 1.3 and FHWM diameters of 256 nm × 327 nm, corresponding to an effective size of 181 nm × 231 nm when corrected for two-photon absorption imaging.

while the electric-field polarization vector was rotated. In these measurements we rotated the half-wave plate through 360°, which corresponded to turning the direction of the electric-field polarization through 720°. The polarization direction repeats itself every 180° (an a.c. field polarized along an angle ϕ is indistinguishable from one polarized along an angle $\phi + 180°$), so we expect to see a modulation in the optical resolution with a period of 180°. The results in Fig. 3 show this behaviour and were inferred from individual line scans performed across one of the gaps between adjacent fingers. The red curve is a least-squares fit to the data, and the fitting function is the diameter of an ellipse drawn at a variable angle to one of its principal axes. The upper error bar represents one standard deviation (31 nm) between the fit and the data, and the lower error bar indicates the measurement error for each data point (±17 nm). The fluctuations in the data can be attributed to small variations in the beam-pointing introduced by rotating the half-wave plate. The fitted curve implies polarization-dependent minimum and maximum resolutions of 122 nm and 240 nm, respectively (a ratio of 1.97).

The theoretical formulism presented in ref. 1 allows us to partially explain the experimental results. In our system we expanded the beam to moderately overfill the pupil of the objective lens used to focus light into the super-SIL, giving a beam diameter (defined at the $1/e^2$ intensity points) of 6.2 mm at the entrance of the 6-mm-diameter pupil. In the silicon super-SIL imaging configuration the maximum useful NA of the objective lens is 0.29, because refraction by the super-SIL increases the NA by a factor of n^2, up to a maximum value of the refractive index of silicon (3.48). By overfilling our 0.55 NA lens we therefore ensured an approximately uniform radial irradiance distribution immediately before the super-SIL. Consequently, the focusing of the system can be understood, to a first approximation, by assuming an incident beam composed of linearly polarized plane waves. For super-SIL imaging we have NA = 3.48, corresponding to the near-infrared refractive index of silicon, and Fig. 4 shows the irradiance distributions calculated for this NA in the $x-z$, $x-y$ and $y-z$ planes, where $x-y$ is the focal plane and the z axis is the optical axis of the system. In these calculations the incident beam was polarized along the y axis and the results indicate that the PSF is extended in the direction parallel to the incident polarization vector by a factor of 1.3. Qualitatively, this asymmetry in the spot size is consistent with our results, which show that, when scanning over a sharp silicon–metal edge, the best resolution is obtained when the beam is polarized parallel to the edge. Under these conditions the width of the PSF is minimized in the scanning direction, giving a more rapid transition in the detected signal as the spot passes over the edge, as observed experimentally.

Although the direction of the extension of the focal spot size is consistent with experiment, a comparison of the resolution values determined from our line scans with the focal-plane irradiance calculated from ref. 1 indicates two discrepancies. One is the absolute size of the PSF inferred from the resolution measurement and the other is the ratio between the PSF widths in the x and y directions. Both differences may be explained by the fact that the presence of an interface near the focal plane can further increase the ellipticity of the focal spot[12]. Detailed modelling of light tightly focused by a glass super-SIL (ref. 13) has predicted an ellipticity in excess of 1.7 at an air–glass interface, and a decrease in the spot full-width at half-maximum (FWHM) perpendicular to the electric-field direction to below the conventional diffraction-limited value of $0.51\lambda/\mathrm{NA}$ (Sparrow's criterion, where λ is the wavelength). In our experiment the light is focused to the 300-nm-thick device layer of a silicon integrated circuit, which forms an interface with an oxide, poly-silicon or metal layer, depending on the precise location being imaged. It is probable that this interface is responsible for enhancing the ellipticity of the focal spot shape beyond the values predicted for focusing in bulk silicon; however, three-dimensional details of the device structure are not available but would be necessary for a rigorous calculation of the focal-plane field distribution. The minimum PSF width of 120 nm is substantially lower than the 181-nm FWHM of the calculated PSF (taking into account the effective $\sqrt{2}$ reduction in the PSF width caused by two-photon excitation). As well as the effect of a refractive-index interface near the focal plane, the irradiance distribution of the illumination beam may also be responsible for reducing the PSF width to below the expected value. Vector-field calculations carried out for tightly focused beams show a strong sensitivity of the focal-spot size and shape to the incident spatial irradiance distribution and polarization state, which is capable of reducing the spot size by approximately a further factor of 0.7 beyond the conventional (scalar) diffraction limited value[14,15]. The greater apparent polarization asymmetry observed experimentally in the PSF may also be a result of the same effect; the analysis presented in ref. 14 indicates that the reduction in spot size is only observed along the direction normal to the polarization vector, so increasing the rotational asymmetry of the focal spot. The incident spatial irradiance distribution and polarization state are strongly modified by the significant differences in the Fresnel transmission coefficients for radial and azimuthal polarizations at the spherical surface of the solid immersion lens, and across the gap between the solid immersion lens and the substrate[11]; these effects could also contribute to the polarization asymmetry reported here. Other physical processes, for example plasmon excitation in the metal edge by the tightly focused rays, may also play a part in modifying the apparent PSF, but remain untested at present.

We anticipate that polarization diversity imaging (where multiple images of the same object are obtained for different polarization states) combined with suitable image processing techniques will yield images with resolutions in all directions that substantially surpass the conventional diffraction-limited value. In biological imaging, where the highest resolutions are obtained at visible wavelengths that are strongly scattered and are more damaging to cells, the possibility of improving resolutions at longer wavelengths by using polarization diversity imaging holds great potential. Polarization diversity imaging is also becoming established as a tool for revealing hidden structure in biological

samples[16], and consequently it could be possible to use multiple images acquired under high-NA focusing both to improve the imaging resolution and obtain structural information about a sample. Finally, we note that although nonlinear microscopy is described in our demonstration, polarization-resolved imaging offers the same benefits to all commonly used variants of linear confocal microscopy.

Received 11 November 2007; accepted 22 January 2008; published 9 March 2008.

References

1. Richards, B. & Wolf, E. Electromagnetic diffraction in optical systems II. Structure of the image field in an aplanatic system. *Proc. R. Soc. London A* **253,** 358–379 (1959).
2. Dorn, R., Quabis, S. & Leuchs, G. The focus of light—linear polarization breaks the rotational symmetry of the focal spot. *J. Mod. Opt.* **50,** 1917–1926 (2003).
3. Bahlmann, K. & Hell, S. W. Depolarization by high aperture focusing. *Appl. Phys. Lett.* **77,** 612–614 (2000).
4. Flagello. D. G. & Milster, T. D. High-numerical-aperture effects in photoresist. *Appl. Opt.* **36,** 8944–8951 (1997).
5. Terris, B. D., Mamin, H. J., Rugar, D., Stundenmund, W. R. & Kino, G. S. Near-field optical data storage using a solid immersion lens. *Appl. Phys. Lett.* **65,** 388–390 (1994).
6. Born, M. & Wolf, E. *Principles of Optics* 7th edn (Cambridge Univ. Press, Cambridge, 1999).
7. Ippolito, S. B., Goldberg, B. B. & Ünlü, M. S. High spatial resolution subsurface microscopy. *Appl. Phys. Lett.* **78,** 4071–4073 (2001).
8. Xu, C. & Denk, W. Two-photon optical beam induced current imaging through the backside of integrated circuits. *Appl. Phys. Lett.* **71,** 2578–2580 (1997).
9. Ramsay, E., Pleynet, N., Xiao, D., Warburton, R. J. & Reid, D. T. Two-photon optical-beam-induced current solid-immersion imaging of a silicon flip chip with a resolution of 325 nm. *Opt. Lett.* **30,** 26–28 (2005).
10. Ramsay, E. *et al*. Three-dimensional nanoscale subsurface optical imaging of silicon circuits. *Appl. Phys. Lett.* **90,** 131101 (2007).
11. Ippolito, S. B., Goldberg, B. B. & Ünlü, M. S. Theoretical analysis of numerical aperture increasing lens microscopy. *J. Appl. Phys.* **97,** 053105 (2005).
12. Novotny, L. & Hecht, B. *Principles of Nano-Optics* (Cambridge Univ. Press, New York, 2006).
13. Karrai, K., Lorenz, X. & Novotny, L. Enhanced reflectivity contrast in confocal solid immersion lens microscopy. *Appl. Phys. Lett.* **77,** 3459–3461 (2000).
14. Quabis, S., Dorn, R., Eberler, M., Glöckl, O. & Leuchs, G. Focusing to a tighter spot. *Opt. Commun.* **179,** 1–7 (2000).
15. Sales, T. R. M. Smallest focal spot. *Phys. Rev. Lett.* **81,** 3844–3847 (1998).
16. Yao, G. & Wang, L. V. Two-dimensional depth-resolved Mueller matrix characterization of biological tissue by optical coherence tomography. *Opt. Lett.* **24,** 537–539 (1999).

Acknowledgements

The authors would like to acknowledge the support of the UK Engineering and Physical Sciences Research Council (EPSRC) under grant number EP/C509765/1. One of the authors (K.A.S.) acknowledges financial support from the EPSRC under a doctoral training award. The support of Credence Inc. is also gratefully acknowledged.
Correspondence and requests for materials should be addressed to D.T.R.

Author contributions

K.A.S. and E.R. performed the experiments. R.J.W. and D.T.R. conceived the project. K.A.S. and D.T.R. analysed the data. All the authors contributed to the writing of the paper.